Journal of Hazardous Materials 424 (2022) 127362

Contents lists available at ScienceDirect

Journal of Hazardous Materials

journal homepage: www.elsevier.com/locate/jhazmat

Research Paper

Superhigh co-adsorption of tetracycline and copper by the ultrathin g-C_3N_4 modified graphene oxide hydrogels

Yiping Feng[a,*], Guang Chen[a], Yijian Zhang[a], Daguang Li[a], Chen Ling[b], Qiaoying Wang[c], Guoguang Liu[a]

[a] Guangzhou Key Laboratory Environmental Catalysis and Pollution Control, Guangdong Key Laboratory of Environmental Catalysis and Health Risk Control, School of Environmental Science and Engineering, Institute of Environmental Health and Pollution Control, Guangdong University of Technology, Guangzhou 510006, China
[b] College of Biology and the Environment, Nanjing Forestry University, Nanjing 210037, China
[c] Shanghai Institute of Pollution Control and Ecological Security, State Key Laboratory of Pollution Control and Resource Reuse, School of Environmental Science and Engineering, Tongji University, Shanghai 200092, China

ARTICLE INFO

Editor: Dr. H. Artuto

Keywords:
Tetracycline
Copper
Co-adsorption
Ultrathin g-C_3N_4
Graphene oxide hydrogels

ABSTRACT

Development of economic and efficient absorbent for the simultaneous removal of antibiotics and heavy metals is needed. In this study, a three-dimensional porous ultrathin g-C_3N_4 (UCN) /graphene oxide (GO) hydrogel (UCN-GH) was prepared by co-assembling of UCN and GO nanosheets via the facile hydrothermal reaction. Characterizations indicated that the addition of UCN significantly decreased the reduction of C═O and O-C═O related groups of GO during the hydrothermal reaction and introduced amine groups on UCN-GH. The UCN-GH exhibited excellent ability on the co-removal of Cu(II) (q_{max} = 2.0–2.5 mmol g^{-1}) and tetracycline (TC) (q_{max} = 1.2–3.0 mmol g^{-1}) from water. The adsorption capacities were increased as UCN mass ratio increasing. The mutual effects between Cu(II) and TC were examined through adsorption kinetics and isotherm models. Characterizations and computational chemistry analysis indicated that Cu(II) is apt to coordinate with the amine groups on UCN than with oxygen groups on GO, which accounts for the enhanced adsorption ability of UCN-GH. In the binary system, Cu(II) acts as a bridge between TC and UCN-GH enhanced the removal of TC. The effects of pH and regular salt ions on the removal of Cu(II)/TC were examined. Moreover, the prepared UCN-GH also showed comparable co-adsorption capacities in practical water/wastewater.

1. Introduction

For a real water environment, the combined pollution of antibiotics and heavy metals has received considerable attention in recent years (Han et al., 2020). It has been determined that antibiotics and heavy metal ions both pose great threats to human health and the environment (Rodriguez-Mozaz et al., 2015; Mishra et al., 2019). Antibiotics and heavy metals have been widely used in the livestock farming field as animal medicines and growth promoters, which as mixtures are finally excreted to the environment (Liu et al., 2019). In addition, industrial wastewater centralization also allowed the combined pollution of antibiotics and heavy metals in surface or groundwater (Schwarzenbach et al., 2006). Generally, due to the easy complexation of antibiotics with heavy metal ions, both compounds have more complicated behaviors in the aquatic environment (Poole, 2017). Moreover, recent studies have shown that the combined toxicities of antibiotics and heavy metal ions are generally higher than their individual toxicities (Zhang et al., 2012; Wang et al., 2021b). In light of this, it is imperative to develop effective treatment methods for eliminating antibiotics together with heavy metals from water.

Various treatment methods have been applied for the removal of antibiotics and heavy metals individually from wastewater, including advanced oxidation (Wang and Zhuan, 2020), chemical precipitation (Yang et al., 2015), adsorption (Ling et al., 2013; Zhu et al., 2018; Zhao et al., 2019), and membrane filtration (Ganiyu et al., 2015). Among these methods, adsorption has been considered as a facile and effective technique due to its low cost, easy operation, and high removal efficiency for both organic and inorganic chemicals. In addition, increasing efforts have also been devoted to the co-adsorption of antibiotics and heavy metals using various adsorbents (Ling et al., 2013; Zhu et al., 2018; Li et al., 2019). However, these traditional adsorbent materials, including activated carbon (Xu et al., 2021), polymer resins (Ling et al.,

---

* Corresponding author.
E-mail address: ypfeng@gdut.edu.cn (Y. Feng).

https://doi.org/10.1016/j.jhazmat.2021.127362
Received 10 August 2021; Received in revised form 17 September 2021; Accepted 25 September 2021

2013), metal oxides (Huang et al., 2017), and minerals (Wang et al., 2008) suffered several limits, including low adsorption capacities and efficiencies, as well as the difficulty in separation and reuse. Therefore, it is needed to design the new adsorbents with functionalized groups for the co-elimination of antibiotics and heavy metals from water.

Due to the high specific surface area and high mechanical strength, the two-dimensional (2D) layered graphene oxide (GO) and its functionalized derivatives have shown great adsorption capabilities for many organic pollutants and heavy metals (Peng et al., 2017; Wang et al., 2018c). To avoid its leaching problems, the graphene-based 3D hydrogels/aerogels were hence constructed (Xu et al., 2010; Gao et al., 2013b). Such graphene-based 3D macrostructures have large adsorption capacity and were able to be separated facilely from water (Gao et al., 2013a). In addition, due to the distribution of oxygen-containing functional groups (e.g., –COOH and –OH) on GO, graphene-based 3D hydrogels can be modified easily, which greatly extended their environmental application potentials (Yousefi et al., 2019). It has been demonstrated that the materials with amine groups (–NH_2, –NH–) modification possessed higher adsorption affinities toward many heavy metals and organic pollutants through coordination and hydrogen bonding / electrostatic attraction (Ling et al., 2013, 2018; Repo et al., 2013), respectively. Therefore, the construction of the amine-modified graphene hydrogels would also have excellent potentials for the co-adsorption of antibiotics and heavy metals.

Chemical modifications were typically used to introduce amine groups onto absorbents (Ling et al., 2013; Zhu et al., 2018), which poses secondary pollution, high cost, and difficult operation problems, thus restricting their usage. Graphitic carbon nitride (g-C_3N_4), a metal-free organic polymeric material, has been widely developed as photocatalytic materials (Xie et al., 2018; Ding et al., 2017). Moreover, due to the desired surface area, nontoxicity, reliable stability, and low cost, g-C_3N_4 has increasingly become a promising adsorption material (Hu et al., 2015; Cai et al., 2017). Especially, the basic tectonic units of g-C_3N_4 are triazine and tri-s-triazine/heptazine, both of which result in the rich of amine groups (–NH_2, –NH–, and =N–) on g-C_3N_4 materials (Ong et al., 2016). These amine groups would also ensure the great adsorption capabilities of g-C_3N_4 for many heavy metals and organic pollutants (Hu et al., 2015; Cai et al., 2017). In addition, the self-assembly 3D macrostructures of g-C_3N_4 and GO could be easily constructed through hydrothermal reaction due to their good compatibility (Tong et al., 2015). The rich surface functional groups like –OH, –COOH, and -NH_2 not only enable the excellent water stability of the g-C_3N_4-GO 3D macrostructures but also could serve as effective adsorption sites for pollutants (Wang et al., 2017). Moreover, the fabrication of g-C_3N_4 into 3D macrostructures resolved the separation problem and hence would greatly facilitate its practical applications in the co-removal of heavy metals and organics.

In this study, the ultrathin g-C_3N_4 modified graphene 3D porous hydrogel was successfully synthesized by a facile one-step hydrothermal method (Tong et al., 2015; Wang et al., 2017). Such a 3D porous hydrogel was rich in multi-functional groups (such as amino, carboxyl, and hydroxyl groups), and therefore suitable for the co-adsorption removal of antibiotics and heavy metals from water. Tetracycline (TC), as one of the most widely used antibiotics, and copper ions, Cu(II), as a typical heavy metal, were used to evaluate the co-adsorption abilities of the prepared 3D porous hydrogel. Previous studies have demonstrated that the co-presence of TC and Cu(II) would mutually change their interaction behaviors toward adsorbent (Nie et al., 2019; Qin et al., 2018; Wang et al., 2019; Jia et al., 2008). Particularly, it has been reported that Cu(II) as the bridge between TC and adsorbent was able to enhance the removal of TC (Ling et al., 2013; Li et al., 2019; Nie et al., 2019; Qin et al., 2018; Wang et al., 2019; Jia et al., 2008). Hence, we were inspired to explore the co-adsorption performance of UCN-GH on TC and Cu(II), which is of great significance for providing foundational knowledge for the potential use of UCN-GH in treating combined pollutants from wastewater. Through batch adsorption experiments, the influences of g-C_3N_4 contents, pH, and ionic strength on the co-adsorption efficiencies were systematically evaluated. The adsorption mechanism was further investigated by Fourier transformation infrared spectrum (FT-IR), X-ray photoelectron spectroscopy (XPS), and computational chemistry analysis.

2. Materials and methods

2.1. Materials

Tetracycline and dicyandiamide were purchased from Aladdin (Shanghai, China).

Natural graphite flake (50 mesh) was purchased from Qingdao Tianhe Graphite Co. Ltd. Sulfuric acid (H_2SO_4, 98 wt%), cupric chloride ($CuCl_2$), hydrogen peroxide (H_2O_2, 30 wt%), hydrochloric acid (HCl), and potassium permanganate ($KMnO_4$) of analytical grade were obtained from Tianjin Kewei Reagent Factory (Tianjin, China). Deionized (DI) water prepared from a Milli-pore Milli-Q system (>18 mΩ cm) was used for solution preparation.

2.2. Preparation of g-C_3N_4 modified graphene hydrogel

2.2.1. Preparation of graphene oxide (GO)

Graphene oxide (GO) was prepared using a modified Hummers' method (Marcano et al., 2010). Briefly, 1.0 g of graphite (50 mesh) was firstly mixed with 200 mL of concentrated H_2SO_4: H_3PO_4 (180 mL: 20 mL). After 9.0 g of $KMnO_4$ was introduced, the mixture was stirred at 300 rpm for 6 h at 50.0 ± 0.2 °C. Then, 20 mL of 30% H_2O_2 was added drop by drop, followed by heating at 50.0 ± 0.2 °C for 3 h. After cooling to room temperature, the obtained mixture was centrifuged and washed with 5% HCl and DI water several times. The obtained GO was further purified by dialysis in DI water using a 5 kDa cellulose membrane for 7 days until the concentration of Cl^- was at trace level.

2.2.2. Preparation of the ultrathin g-C_3N_4 (UCN)

The ultrathin g-C_3N_4 (UCN) nanosheets were prepared through a thermo-polymerization method as described in our previous works (Xie et al., 2018; Wang et al., 2018a). Briefly, 3.0 g of dicyandiamide and 15.0 g of ammonium chloride (NH_4Cl) were mixed and dissolved in 20 mL of DI water by stirring at 80.0 ± 0.2 °C. The solution was then transferred into an alumina crucible, sealed with alumina foil, and heated at 550 °C for 3 h at a heating rate of 2.7 °C min^{-1}. After cooling to room temperature, the obtained UCN powder was collected and finely grounded for further use. As demonstrated by the transmission electron microscope (TEM) in Fig. S1, the UCN has a 2D ultrathin lamellar structure.

2.2.3. Synthesis of g-C_3N_4 modified graphene oxide hydrogel (UCN-GH)

The self-assembled graphene oxide hydrogel (GH) and g-C_3N_4 modified GH (UCN-GH) were prepared via a convenient one-step hydrothermal method (Xu et al., 2010; Wang et al., 2017). Typically, a certain amount of UCN nanosheets (with the mass ratio of 0–35%) was added to 30 mL of GO suspensions (4 mg mL^{-1}), and then the solution was mixed through ultrasonic treatment for 30 min. GO has high dispersity in water due to the abundant oxygen-functional groups (Feng et al., 2017), therefore, the uniformly dispersed UCN-GO hetero-aggregation hybrids can be formed. Then, the homogeneous UCN-GO hybrids solutions were transferred into a 100-mL Teflon-lined autoclave and heated at 180 °C for 6 h. After naturally cooling to room temperature, the self-assembled 3D graphene oxide hydrogel (GH) and UCN modified GH (UCN-GH) were obtained.

2.3. Characterization

The microstructures of the prepared GH and UCN-GH were observed by a Hitachi S4800 scanning electron microscope (SEM). The elemental compositions of samples were characterized by an energy dispersive spectroscopy (EDS) equipped on the SEM. The chemical components and valence states of the samples were analyzed using X-ray photoelectron spectroscopy (XPS) on a Thermo VG ESCALAB 250 spectrometer with Al Kα radiation. Fourier transform infrared spectra (FT-IR) was carried out on a Thermo Nicolet 6700 spectrometer with the samples dispersed in KBr. The crystal structure of the obtained materials was characterized by X-ray diffraction (XRD, Bruker D8 ADVANCE) with Cu Kα radiation. Nitrogen adsorption-desorption isotherms were recorded on an SA3100 surface area analyzer (Beckman Coulter, USA) to determine the specific surface areas of the as-prepared samples. Coordination structures were optimized based on Density-Functional-Theory (DFT) which was processed using Gauss view v5.0 and Gaussian 09 with the detailed information in SI.

2.4. Adsorption experiments

Batch adsorption experiments were performed by mixing 0.10 g (dry weight) of hydrogel with 50 mL of tetracycline (TC) and Cu(II) solutions at predetermined initial concentrations in 150-mL glass flasks. The initial pH of solutions was all adjusted to 5.0 by 0.2 mol L^{-1} HCl or NaOH. The flasks were kept on a rotary shaker at 140 rpm and 25 ± 0.2 °C (298 K). At the prespecified sampling time, the residual concentrations of TC in the solutions were determined at 360 nm by a UV–vis spectrophotometer (Mapada 3200 UV–Vis, Shanghai, China), and the residual concentrations of Cu(II) were measured by an atomic absorption spectrophotometer (AAS, Thermo, USA). All adsorption experiments were conducted at least in duplicate to obtain an average value.

Adsorption kinetics of TC and Cu(II) on UCN-GH with UCN ratio varying from 0 to 35% was examined with 0.2 mmol L^{-1} of TC and 2.0 mmol L^{-1} of Cu(II). Pseudo-first-order rate kinetics and pseudo-second-order kinetics were applied to interpret the kinetics parameters, as described in Eqs. (1) and (2),

$$\mathrm{In}(q_e - q_t) = \mathrm{In}\, q_e - k_1 t \tag{1}$$

$$\frac{t}{q_t} = \frac{1}{k_2 q_e{}^2} + \frac{t}{q_e} \tag{2}$$

Where q_e and q_t are the adsorption amount (mmol g^{-1}) during equilibrium and time t. k_1 and k_2 (g $mmol^{-1}$ min^{-1}) are the constants associated with the adsorption rate obtained from the corresponding equation. $h = k_2 q_e{}^2$ was defined as the initial adsorption rate constant.

Adsorption isotherms of TC and Cu(II) on UCN-GH with UCN content of 0.3 were conducted in their sole and binary systems. In the binary systems, the initial concentrations of Cu(II) were set as 0–6.0 mmol L^{-1} and TC concentration was fixed at 0.2 mmol L^{-1}, or the initial concentrations of was TC set as 0–2.0 mmol L^{-1} and Cu(II) concentration was fixed at 2.0 mmol L^{-1}. After 24 h incubation, the residual concentrations of TC and Cu(II) in the solutions were determined, respectively. The equilibrium adsorption amount (q_e, mmol g^{-1}) was calculated by Eq. (3). Langmuir and Freundlich models were respectively used to fit the adsorption isotherms, as present in Eqs. (4) and (5).

$$qe = \frac{(C_o - C_e)V}{m} \tag{3}$$

$$q_e = \frac{b q_{\max} C_e}{1 + b C_e} \tag{4}$$

$$q_e = K_f C_e^{\frac{1}{n}} \tag{5}$$

Where C_0 and C_e are the initial and equilibrium concentration (mmol L^{-1}) of TC and Cu(II), m is the dry weight of GH or UCN-GH (g), V is the volume of the solution (L), b is the Langmuir sorption constant (L $mmol^{-1}$), and q_{max} is the adsorption capacity (mmol g^{-1}). K_f and n are the Freundlich constant isotherm parameters that represent relative capacity and adsorption intensity, respectively.

3. Results and discussion

3.1. Characterization

With the hydrothermal technique, the ultrathin g-C_3N_4 (UCN) modified graphene oxide hydrogels (GH) can be fabricated easily with controllable shape and size. Fig. 1a showed that both pristine GH and UCN-GH are cylindrical in shape and black in color. The size of the prepared GH and UCN-GH is ca. 0.5 cm in radius × 1.0 cm in height and ca. 0.6 cm in radius × 1.2 cm in height, respectively. The prepared GH and the UCN-GH both possess strong mechanical properties. After freeze-dried, the morphology of pure GH (Fig. 1b) and UCN-GH (Fig. 1c) was then observed by scanning electron microscopy (SEM). It can be seen that both GH and UCN-GH possess a well-defined and interconnected 3D porous microstructure (Xu et al., 2010; Tong et al., 2015). EDS analysis of UCN-GH revealed the presence of the C, O, and N elements (Fig. S2), indicating that the UCN nanosheets are distributed uniformly in the UCN-GH composites (Tong et al., 2015).

Fig. 1d shows the typical FT-IR spectrum of pure GO, UCN, GH, and UCN-GH composites. There are many oxygen-containing groups in GO, including O-H (3423 cm^{-1}), C=O (1724 cm^{-1}), C-OH (1276 cm^{-1}), and C-O (1050 cm^{-1}) (Feng et al., 2019). Hydrothermal reduction greatly reduced the oxygen-functional groups in GH (Tong et al., 2015; Wang et al., 2017). For pure UCN, the broad vibration bands at 1000–1700 cm^{-1} in pure UCN are attributed to the C-N stretching vibrations in the C-N heterocycles. The peak at 814 cm^{-1} corresponds to the vibration mode of the s-triazine unit, and the broad vibration bands at 3000–3500 cm^{-1} are related to the stretching vibrations of the C-OH and N-H groups (Wang et al., 2018b). FT-IR spectra of UCN-GH are similar to those of pure UCN, which has oxygen-containing groups like O-H (3433 cm^{-1}) (Tong et al., 2015; Wang et al., 2017). In addition, the UCN-GH composite did not exhibit any new characteristic peaks, implying that the hybridization did not create any new molecular bonds (Wang et al., 2017). Fig. 1e represents the X-ray diffraction (XRD) patterns of GH, UCN, and UCN-GH. GH exhibited a very broad peak centered at $2\theta = 24.2°$, indicating that GO nanosheets were reduced and restacked during the hydrothermal process(Zeng et al., 2015). UCN nanosheets have two distinct diffraction peaks at $2\theta = 27.5°$ (002) and 13.0° (100), corresponding to the graphitic structure and the in-plane ordering of tri-s-triazine units of g-C_3N_4. Wang et al. (2009) For the as-prepared UCN-GH sample, the characteristic peak at $2\theta = 27.5°$ indicated the presence of well-crystalline g-C_3N_4 structure in the composites. However, the peak at $2\theta = 27.5°$ of UCN-GH became wider than that of pure UCN might due to the overlapping with the broad peak at $2\theta = 24.2°$ of GH. Meanwhile, the characteristic peak of GO at $2\theta = 11.1°$ also appeared indicating that GO is partially converted into reduced GO (rGO) during the hydrothermal process for UCN-GH samples (Tong et al., 2015).

Additionally, XPS was used to analyze the elemental composition and chemical state of the samples. The XPS survey spectrum of GO, UCN, GH, and UCN-GH composites was displayed in Fig. 1f. GH contains C and O elements, while UCN-GH contains C, N, and O elements. The O1s spectra in Fig. 1g also revealed that the content of oxygen element in C=O and O-C=O of UCN-GH are 2 and 3 times higher than that of GH, respectively. This result implied that UCN-GH has more oxygen-functional groups (e.g., -COOH) as active sites than pure GH. However, Fig. S3 and Table S1 showed that the micropores volume and surface area of UCN-GH is much lower than that of GH prepared in the same way, while the pore size of UCN-GH (17.75 nm) is much larger than that of GH (2.77 nm). This phenomenon can be assigned to the attachment of g-C_3N_4 nanosheets on GO, which enhances the thickness of the composites (Tong et al., 2015; Wang et al., 2017). In conclusion, the results of characterization indicated that the addition of UCN not only provided amine groups but also reduced the reduction of oxygen-functional

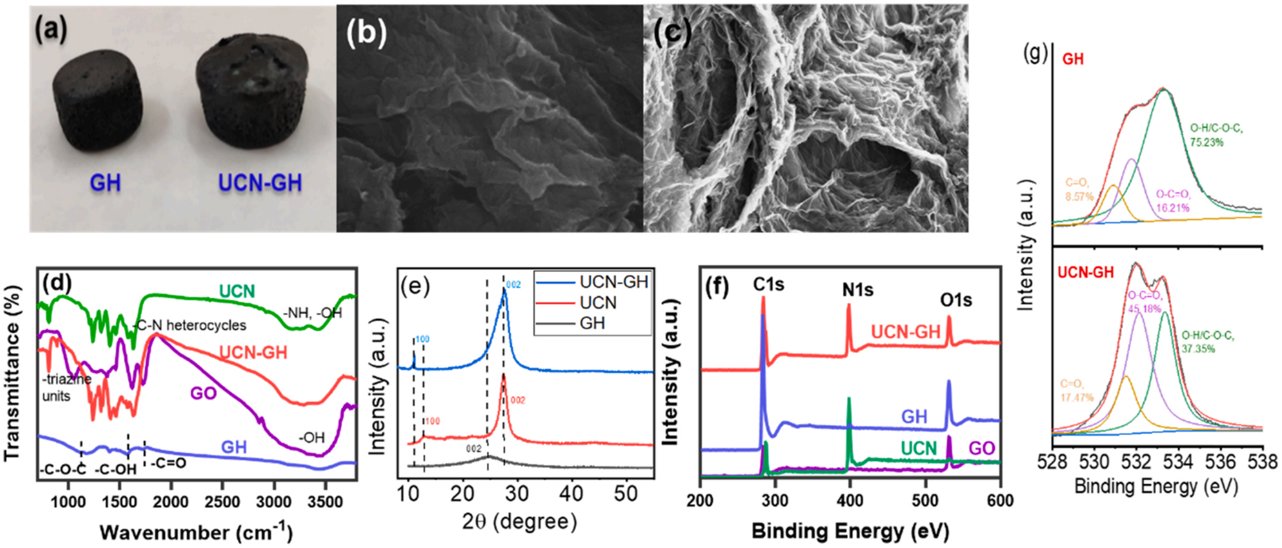

Fig. 1. Characterization of GH and UCN-GH. (a) Photograph of GH and UCN-GH, SEM images of pure GH (b) and UCN-GH (c), (d) FT-IR spectra, (e) XRD spectra and (f) XPS survey spectra of UCN, GO, GH, and UCN-GH, and (g) XPS-peak-fitting analysis of the average oxygen element content of GH and UCN-GH.

groups on GO during the hydrothermal reaction, both of which would be beneficial to the adsorption of pollutants.

3.2. *Co-adsorption behaviors*

3.2.1. *Co-adsorption performance of GH and UCN-GH*

The adsorption of TC and Cu(II) by pure GH, UCN-GH, and UCN powder with the single presence of TC or Cu(II), or with the co-presence of them were compared, as shown in Fig. 2. For the single system (SS), TC was adsorbed onto both pure GH and UCN-GH through π-π interaction and cation–π bonding electrostatic interaction (Gao et al., 2012). The adsorption capacity (q_e) for TC-SS on UCN-GH (ca. 0.4 mmol g^{-1}) was slightly increased than that on pure GH (i.e., ca. 0.3 mmol g^{-1}), which might be because of the favorable electrostatic interaction between negatively charged groups of TC and the protonated amine groups (–NH_2, –NH–, and =N–) on g-C_3N_4 sheets (Zhu et al., 2018; Ong et al., 2016). The H-bonding interaction between –OH on TC and –NH_2 on UCN also contributes to TC adsorption on UCN-GH (Yang et al., 2011). In addition, in the single system, the adsorption of Cu(II) onto UCN-GH was significantly enhanced, which was 3.41 times higher compared to the q_e of Cu(II) on the pure GH due to the strong coordination interaction between Cu(II) and amine groups on g-C_3N_4 materials (Ong et al., 2016; Xing et al., 2015), as well as the oxygen-functional groups (e.g., –COOH and –OH) on graphene plane. The adsorption capacities of TC and Cu(II) on pure UCN powder were respectively determined to be ca. 0.03 and 0.18 mmol g^{-1}, which are much lower than that on GH as well as UCN-GH. The poor absorption ability of UCN power might be due to its small specific surface area as well as the poor dispersion in water (Tong et al., 2015; Wang et al., 2017).

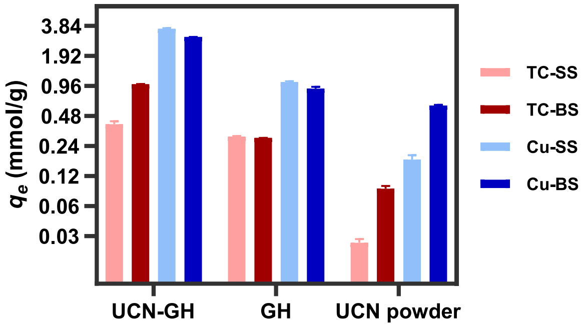

Fig. 2. Adsorption capacities of TC and Cu(II) on UCN-GH, GH, and UCN powder in TC, Cu(II) single existence system (SS), or in the binary system (BS) with the coexistence of TC and Cu(II). Experimental conditions: hydrogel mass is 0.2 g L^{-1}, initial TC and Cu(II) concentrations are 0.2 and 2.0 mmol L^{-1}, the temperature is 25 °C, pH 5.0, and the contact time was set as 24 h.

For the binary system (BS) where TC coexisted with Cu(II), TC adsorption onto pure GH was changed slightly, while Cu(II) adsorption was suppressed than in their single systems. Similarly, the adsorption of Cu(II) onto UCN-GH was also inhibited by TC in a binary system. The Cu (II) adsorption reduction in BS is probably because the strong coordination of Cu(II) with TC reduce its interaction with the functional groups (e.g., -COOH and -NH) in the sorbent, and the formation of TC-Cu(II) complex change the surface charge and molecular size of Cu(II) (Zhu et al., 2018). Meanwhile, the co-presence of TC would inhibit Cu(II) adsorption through pore blocking, competing, and screening interaction sites in the sorbent (Kang et al., 2010). However, the adsorption of TC onto UCN-GH was enhanced by Cu(II) in the binary system, e.g., the q_e for TC on UCN-GH with the presence of Cu(II) was ca. 1.0 mmol g^{-1}, which was 2.51 times higher than TC in a single system. This phenomenon was probably ascribed to the bridging effect of surface Cu for TC forming hydrogel-Cu-TC tertiary complexes (Zhu et al., 2018). The results suggested that the introduction of UCN to GO-based hydrogel significantly improved their synergistic co-removal of TC and Cu(II).

3.2.2. *Adsorption kinetics and isotherms*

The adsorption kinetics of TC and Cu(II) in their single or co-presence systems on UCN-GH were investigated. Fig. 3a shows that the adsorption of TC and Cu(II) on UCN-GH was increased with contact time. It was apparent that the adsorption TC reached equilibrium at ca. 100 min while the adsorption equilibrium of Cu(II) is reached at more than 200 min. The kinetic data were further described using pseudo-first-order and pseudo-second-order models and the obtained kinetic parameters were summarized in Table S2. It was notable that the pseudo-second-order model fits better the kinetic data with the higher correlation coefficient R^2 values (0.92–0.98). This result indicated that both TC and Cu(II) adsorption was influenced by chemical mechanisms which were determined by both the surface properties of hydrogels and the transport processes of TC and Cu(II) (Hu et al., 2015). In addition, adsorption kinetics also revealed that the presence of Cu(II) significantly promoted TC adsorption (e.g., $q_{e,\ TC\text{-}SS,\ cal}$= 0.6 mmol g^{-1}, $q_{e,\ TC\text{-}BS,\ cal}$= 1.2 mmol g^{-1}), but TC slightly impeded Cu(II) adsorption (e.g., $q_{e,\ Cu(II)\text{-}SS,\ cal}$= 3.7 mmol g^{-1}, $q_{e,\ Cu(II)\text{-}BS,\ cal}$= 2.8 mmol g^{-1}). Nevertheless,

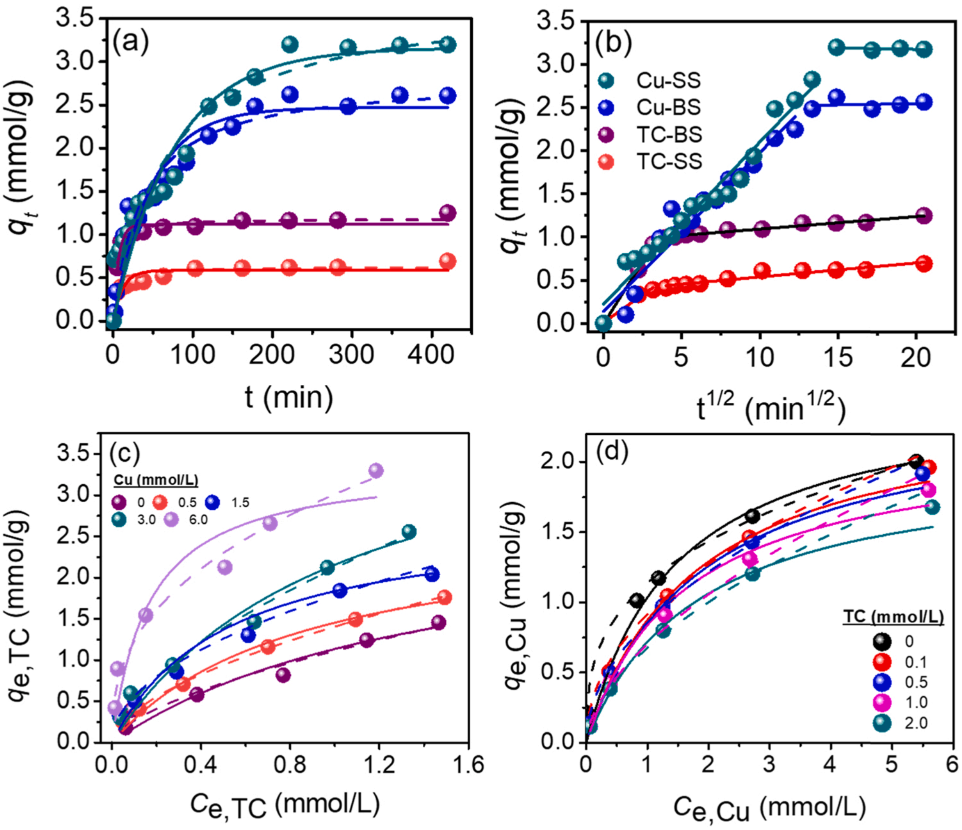

Fig. 3. (a) Adsorption kinetic curves and (b) intraparticle diffusion for the adsorption of TC and Cu(II) on UCN-GH fitting by the first-order kinetic model (solid lines) and second-order kinetic model (dashed lines), experimental conditions: hydrogel mass is 0.2 g L^{-1}, initial Cu(II) and TC concentrations are 2.0 and 0.2 mmol L^{-1}, the temperature is 25 °C, and pH is 5.0. Adsorption isotherms of TC (c) and Cu(II) (d) in single and binary systems fitted by Langmuir model (solid lines) and Freundlich model (dashed lines).

the simulated adsorption rate constant k_2 and the initial adsorption rate constant (h) in the binary system were higher than that in the single system, indicating the faster adsorption in binary systems. On the contrary, the growth of [Cu-TC] complex with increasing molecular size results in pore obstruction; meanwhile, the formation of [Cu-TC] complex also decreased the amount of positively charged Cu(II) and hence reduced its electrostatic attraction with hydrogels, thereby diminished the adsorption of Cu(II) (Qin et al., 2018).

Furthermore, the intraparticle diffusion model was also applied to examine the adsorption behavior of TC and Cu(II) onto UCN-GH in their single or binary systems. As shown in Fig. 3b, the fitting curves of q_t versus $t_{1/2}$ for the adsorption of both TC and Cu(II) were multilinear, indicating that TC and Cu(II) adsorption onto UCN-GH were simultaneously controlled by liquid-film diffusion and intraparticle diffusion (Wang et al., 2021a). The adsorption includes two stages: stage I with a large slope reflects the transport of TC and Cu(II) through the boundary film to the external surface of UCN-GH; stage II with a lower slope was attributed to slow transport of TC and Cu(II) from the external surface into the inner pores of UCN-GH until reach equilibrium (Ma et al., 2021).

In addition, to evaluate the mutual effects of TC and Cu(II) in their co-adsorption process, the adsorption isotherms of TC and Cu(II) onto UCN-GH in their single and binary systems were examined, as shown in Fig. 3c and d. The adsorption of TC at various initial concentrations was all enhanced as the increase of co-present Cu(II) concentrations from 0 to 6.0 mmol L^{-1} (Fig. 3c). Oppositely, the co-presence of TC (0–2.0 mmol L^{-1}) inhibited the adsorption of Cu(II), and the inhibition gradually increased as TC concentration increase (Fig. 3d). Langmuir and Freundlich models were further applied to fit the isotherm data, and the obtained parameters were tabulated in Table S3. The adsorption isotherms of TC and Cu(II) on UCN-GH were well described with the Freundlich model as indicated by the high R^2 (0.956–0.999), indicating that the adsorption of TC and Cu(II) on UCN-GH is likely multilayer adsorption (Saadi et al., 2015). The adsorption affinity ($\underline{K}_f$) of TC onto UCN-GH was gradually enhanced as the co-present Cu(II) concentration increased, which is consistent with the kinetics study. The fitted values of the maximum adsorption amount (q_{max}) of UCN-GH for the co-adsorption of TC and Cu(II) were also simulated, as shown in Table S3. q_{max} for TC showed a positive correlation with the concentration of co-present Cu(II), e.g., $q_{max,\ TC}$ was increased from 0.67 to 2.98 mmol g^{-1} as Cu(II) increased from 0 to 6.0 mmol L^{-1}. Although the co-presence of TC reduced the adsorption of Cu(II), the simulated $q_{max,\ Cu(II)}$ is considerably high (e.g., 2.04 mmol g^{-1}) even with TC at a high concentration of 2.0 mmol L^{-1}. In addition, we have also compared the co-adsorption capacity of other materials on removing TC and Cu(II), as listed in Table S4. Compared to biochar (Wang et al., 2020), resins (Ling et al., 2013; Zhu et al., 2018), alginate beads (Luo et al., 2021), as well as graphene oxide (Zhao et al., 2019), the prepared UCN-GH in the current study displayed exceptional co-adsorption capacities for TC and Cu(II). Particularly, the maximum detected adsorption capacity for TC is 3–10 times higher than that of other adsorbents (Ling et al., 2013; Zhu et al., 2018; Wang et al., 2020). Consequently, the UCN-GH is considered a practicable absorbent with excellent co-adsorption potential for removing TC and Cu(II).

3.3. Effect of ultrathin g-C_3N_4 contents

To better understand the synergistic effect of UCN modification on the co-removal of TC and Cu(II) by GO-based hydrogels, we prepared a series of UCN modified hydrogels under UCN mass concentration ratios ranging from 0 to 0.35. The co-adsorption behaviors of these prepared UCN-GHs on TC and Cu(II) within 6 h are presented in Fig. 4. The adsorption kinetics were also fitted using pseudo-first-order and pseudo-second-order models and the obtained kinetic parameters were listed in Table S5. The pseudo-second-order model indicated that the adsorption capacities ($q_{e,\ TC}$ and $q_{e,\ Cu}$) of both TC and Cu(II) depend on UCN mass contents. Both fitted $q_{e,\ TC}$ and $q_{e,\ Cu}$ increased with enhancing UCN mass contents from 0 to 0.35. At the UCN mass contents of 0.35, both $q_{e,\ TC}$ and $q_{e,\ Cu}$ reached a maximum value of 1.24 and 5.33 mmol g^{-1},

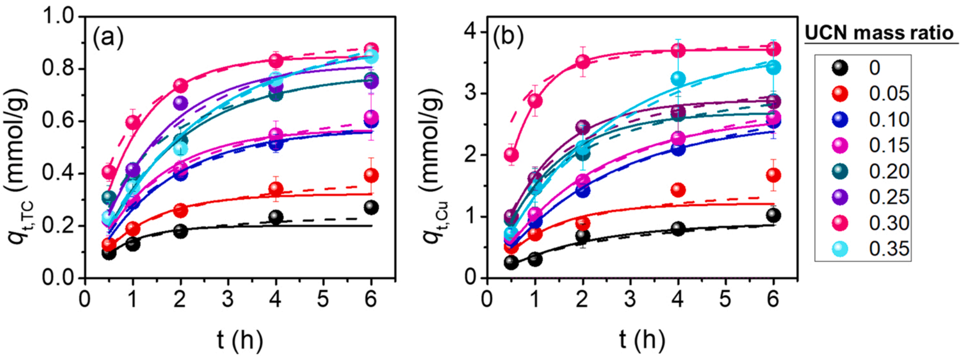

Fig. 4. Effect of ultrathin g-C_3N_4 mass contents (0–0.35) on the adsorption capacities of TC (a) and Cu(II) (b) on UCN-GH in the Cu(II) and TC coexistence system. Experimental conditions: hydrogel mass is 0.2 g L^{-1}, initial Cu(II) and TC concentrations are 2.0 and 0.2 mmol L^{-1}, the temperature is 25 °C, and pH is 5.0.

respectively. For pure GH, $q_{e,\ TC}$ and $q_{e,\ Cu}$ are only 0.26 and 1.15 mmol g^{-1}, respectively. The results indicated that the addition of g-C_3N_4 nanosheets supplied a lot of amine groups for the coordination of Cu(II) and hence increased the adsorption of Cu(II) as well as TC. However, the calculated adsorption rate constant k_2 and the initial adsorption rate constant (h) for both TC and Cu(II) firstly increased and then decreased as UCN mass content increase. For example, when UCN mass content was 0.30, both k_2 and h reached maximum, while as further increasing UCN mass content to 0.35, both k_2 and h decreased. The results might be due to the excessive loading of UCN reduced the specific surface area and micropore size of UCN-GH due to the specific surface area of UCN was much smaller than graphene (Wang et al., 2017), which was also demonstrated by the specific surface measurement (Fig. S3 and Table S1). In addition, excessive UCN also might block the pore of hydrogel and hence hindered the diffusion of TC and Cu(II) into the inside of UCN-GH.

3.4. Effect of pH, ions, and water matrix

Fig. 5a presents the zeta-potentials of UCN-GH under different pH conditions. The zeta-potential of UCN-GH decreased with increasing pH, while isoelectric points (IEPs) of UCN-GH was observed at pH = 5.2. As a result, the surface of UCN-GHs is negatively charged when pH > IEPs due to the ionization of oxygen functional groups (Feng et al., 2017). Furthermore, we examined the co-adsorption of TC and Cu(II) by UCN-GH under pH ranges between 2.0 and 6.0. As shown in Fig. 5b, the adsorption capacity of TC and Cu(II) increased as pH increased from 2.0 to 6.0. When pH < IEPs (pH = 5.2), UCN-GH is positively charged because its surface species were protonated. Consequently, the adsorption capacities of Cu(II) by UCN-GH were low under acidic pH conditions due to the electrostatic repulsion. As pH values increased, the surface charges of UCN-GH became more negative, and the adsorption capacities of Cu(II) significantly increased. At pH > 6.0, the hydrolysis of Cu(II) occurred resulting in the precipitation of Cu(II), and hence the

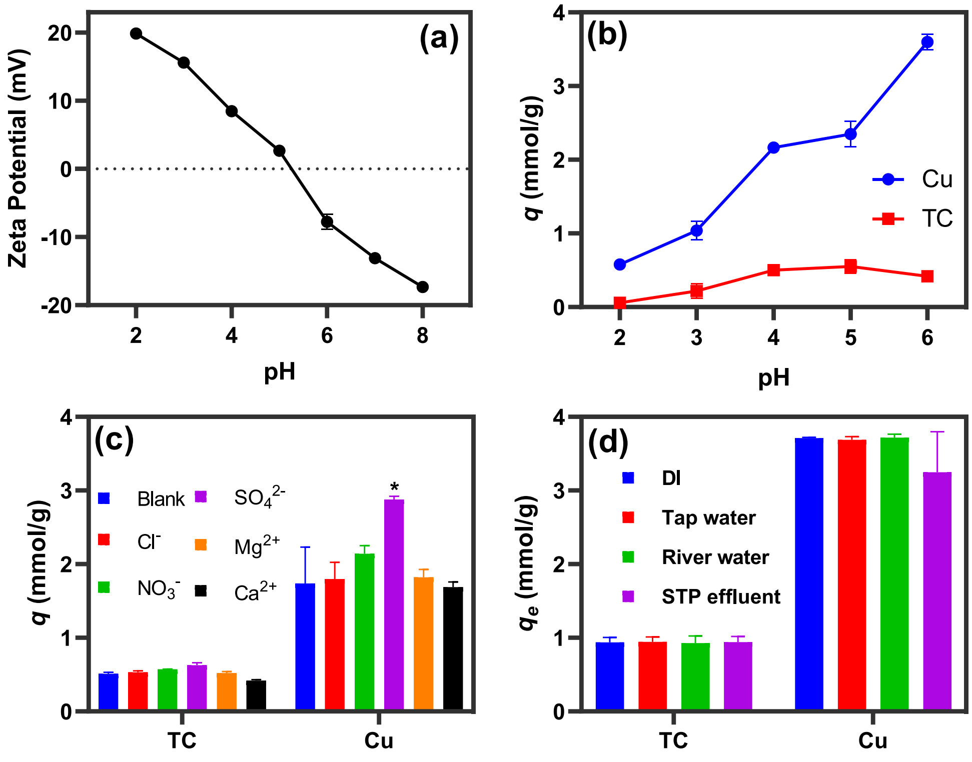

Fig. 5. Zeta-potentials of UCN-GH under different pH values (a), and effects of pH (b), different ions (c), as well as water matrix (d) on the co-adsorption capacities of TC and Cu on UCN-GH. Experimental conditions: C_{TC}= 0.2 mmol L^{-1}, C_{Cu}= 2.0 mmol L^{-1}, C_{anions}= 10.0 mmol L^{-1}, temperature = 25 °C, pH = 5.0, and contact time was 3 h.

adsorption of Cu(II) was not examined at pH > 6.0. The adsorption of TC increased as solution pH increased from 2.0 to 5.0 (Fig. 5b). At pH < 3.3, TC exists in its cationic form, while TC exists as zwitterion between pH 3.3 and 7.7, and changes to anion at pH > 7.7 (Chen et al., 2016). Due to electrostatic repulsion between cationic TC species and positive surface charges on UCN-GH, the adsorption of TC under acidic pH 2.0 and 3.0 is not favored. As pH rises to 4.0 and 5.0, the amount of cationic TC species drops and TC turns to zwitterion in the solution. The electrostatic repulsion between TC and UCN-GH decreased and hence increased TC adsorption. However, the UCN-GH surface is negatively charged at high pH (e.g., pH = 6.0), and TC molecules exist mainly in the anion form. Therefore, the adsorption of TC decreased at pH 6.0 due to electrostatic repulsion. Besides, the equilibrium pH values of solutions after adsorption dropped, probably resulting from H^+ release through ion exchange.

The effect of coexisting typical anions and cations (on the adsorption of TC and Cu(II) on UCN-GH was also examined. As shown in Fig. 5c, the presence of Cl^-, NO_3^-, and Mg^{2+} showed no obvious influence on either TC or Cu(II) removal. However, Ca^{2+} inhibited TC and Cu(II) adsorption, i.e., the adsorption amount of TC and Cu(II) dropped by ca. 20% and 4% with the presence of 10 mmol L^{-1} Ca^{2+}, respectively. Previous studies showed that Ca^{2+} ions can bind with carboxyl functional groups on graphene oxide and hence reduced the electrostatic adsorption of TC-Cu(II) (Zhao et al., 2019). In addition, like [Cu-TC] complex, TC could bind with Ca^{2+} to form [Ca-TC] complex, which possesses lower adsorption affinity with UCN-GH (Li et al., 2019; Parolo et al., 2012). Interestingly, the adsorption of TC and Cu(II) was obviously promoted in the presence of SO_4^{2-} compared to other anions, i.e., the adsorption amount of TC and Cu(II) enhanced by ca. 24% and 66% with the presence of 10 mmol L^{-1} SO_4^{2-}, respectively. The electric double layer compressing by SO_4^{2-} might account for the promoted adsorption (Zhang et al., 2019). A similar phenomenon has been reported in the adsorption of Cu(II) by NH_2-MCM-41 material, where the formation of $[CuSO_4]^0$ species further co-adsorbed with Cu^{2+} to form stable complexes, as well as SO_4^{2-} may even indirectly react with the weakly acidic hydroxyl groups to liberate $-NH_2$ for more TC-Cu(II) adsorption (Lam et al., 2008).

In order to evaluate the technical feasibility of the prepared UCN-GH on the adsorption of the combined contaminants in the aquatic environment, the co-adsorption ability of UCN-GH in different natural water matrices was examined. Fig. 5d presents the co-adsorption capacities of TC and Cu(II) in different water matrices. Obviously, the adsorption amounts of both pollutants were not influenced by the mater matrix, except the adsorption of Cu(II) was slightly reduced in effluent water where natural organic matters (Table S6) compete for the adsorption sites (Wang et al., 2021a). These results indicated that the prepared UCN-GH is suitable for the treatment of TC and Cu(II) contaminated natural surface water or wastewater. We further examined the regeneration and reuse of UCN-GH successively by using 0.1 mol L^{-1} NaOH and 1.0 mol L^{-1} HCl solutions as the desorption agent. As a result, both TC and Cu(II) could be recovered efficiently. In addition, Fig. S4 also showed that UCN-GH had a stable performance for co-removal of Cu(II) and TC after three cycles of adsorption and desorption procedures. Moreover, through column dynamic adsorption experiments, we have also found that the 10% breakthrough volume (10% BTV, L g^{-1}) of UCN-GH is much higher than GH (Table S8). According to references by Khan et al. (2019a, 2019b), we further proposed the simple figure of merit (FOM) as FOM $= \frac{10\%\ BTV(L\ g^{-1})}{Sorbent\ \cos t(USD\ g^{-1})}$ (Table S7). The FOM of UCN-GH is 3.5 times higher than that of pure GH, implying that UCN-GH is more applicable than GH for the co-adsorption of TC and Cu(II) (Khan et al., 2019b).

3.5. Adsorption mechanisms

The XPS spectra of UCN-GH before and after the adsorption of Cu(II) and co-adsorption of TC and Cu(II) are characterized. Fig. S5 shows that UCN-GH contains C, N, and O elements on its surface before adsorption, while a peak of element Cu appeared after the adsorption of Cu(II) or co-adsorption of TC and Cu(II), confirming the adsorption of Cu. The XPS peak fitting of O1s, N1s, and Cu2p are presented in Fig. S6. The N1s spectra of UCN-GH show four peaks located at 398.41, 399.52, 400.60, and 404.13 eV, corresponding to sp^2-bond nitrogen of triazine units (C=N-C), tertiary nitrogen (N-C_3), amino-functional groups (N-H), and special charging effects, respectively (Wang et al., 2018b; Jiang et al., 2016). After Cu(II) uptake, the peak of C=N-C shifted to higher energy (398.78 eV), indicating a reduced electron density of the N atoms due to its interaction with Cu(II) (Ling et al., 2013; Cai et al., 2017). The sp^2-bond nitrogen can provide the coordination sites for Cu(II) because of their lone-pair electrons (Cai et al., 2017). After co-adsorption of TC, the peak of C=N-C shifted to much higher energy (398.80 eV), probably due to the bridging interaction of the N-Cu complex with TC (Ling et al., 2013). The C1s spectra indicated that the binding energy of sp^2-bonded carbon at 288.12 eV (O-C=O/N-C=N) was shifted to + 0.21 and + 0.11 eV after Cu(II) adsorption and TC-Cu(II) co-adsorption, respectively, also indicating a strong interaction between Cu/Cu-TC and C-related functional groups (Zhao et al., 2019; Cai et al., 2017).

The O1s spectra of UCN-GH can be divided into three peaks located at 531.50, 532.12, and 533.35 eV, corresponding to C=O, O-C=O, and O-H/C-O-C, respectively (Luo et al., 2021). After uptake of Cu(II), the binding energies of the O atom in C=O, O-C=O, and O-H/C-O-C were all shifted to higher energies, demonstrating the involution of these groups in Cu adsorption. However, the co-uptake of TC did not lead to an obvious shift of O1s might because the TC molecules have a higher content of oxygen-containing groups (Ling et al., 2013; Li et al., 2019; Luo et al., 2021). For Cu2p spectra, the binding energies of 933.05, 934.98 eV, and 944.04 eV for Cu $2p_{3/2}$, and 954.18 eV for Cu $2p_{1/2}$ in UCN-GH_Cu sample are shifted to 932.37, 934.36 eV, and 941.61 eV for Cu $2p_{3/2}$, and 952.91 eV for Cu $2p_{1/2}$ in UCN-GH_Cu+TC sample, respectively. This result confirmed again that the captured Cu participated in the coordination of TC. In addition, FT-IR spectra (Fig. S7) also showed that the C=O group (1732 cm^{-1}) and -OH/-NH groups (3372 cm^{-1}) were weakened, indicating the interaction between Cu(II) or TC-Cu(II) complex with these oxygen and nitrogen-containing functional groups (Ling et al., 2013).

The interactions among Cu(II) and TC in the aqueous phase, and with the interfaces of CN/GO planes were further investigated by DFT calculations (Ling et al., 2018; Gao et al., 2013b). The obtained coordination configurations were presented in Fig. S8 and the corresponding energy information was shown in Table S8. Generally, the coordination configuration with lower binding energy (ΔE) is considered to be more stable (Song et al., 2012). We first compared the sole interaction of Cu/TC with GO or CN. The positive ΔE implied Cu(II) is hard to be coordinated with the N at the center of CN. Cu(II) is apt to coordinate with the amine groups on the edge of CN and oxygen groups on GO due to both have low ΔE values. Meanwhile, the lower ΔE of CN-edge N-Cu^{2+} than GO-Cu^0 indicates the stronger affinity between Cu(II) and UCN, which is the reason for the enhanced adsorption performance of UCN-GH towards Cu(II). On the contrary, ΔE values also indicated that free TC has minor interaction with CN, resulting in the low adsorption capacity of UCN towards TC. The strong interaction between Cu and TC was also demonstrated, indicating that [Cu-TC] complex of Cu(II) coordinated with O/O of pK_{a2} and O/N of pK_{a1} on TC are more stable with the lower ΔE (Table S8) (Wang et al., 2008). The possible bridging effect of Cu(II) on the adsorption of TC onto UCN-GH was further examined. Clearly, the negative ΔE values in Table S8 well proved the possibility of Cu(II) as the bridge between TC and UCN-GH for TC adsorption (Ling et al., 2018).

Based on the results and the relevant literature, the adsorption mechanism for the co-adsorption of TC and Cu(II) onto UCN-GH was then proposed, as presented in Fig. 6. Firstly, the UCN-GH obtained abundant amine groups from UCN and oxygen-functional groups from GO as active sites for adsorption. Meanwhile, the bulk π systems on UCN

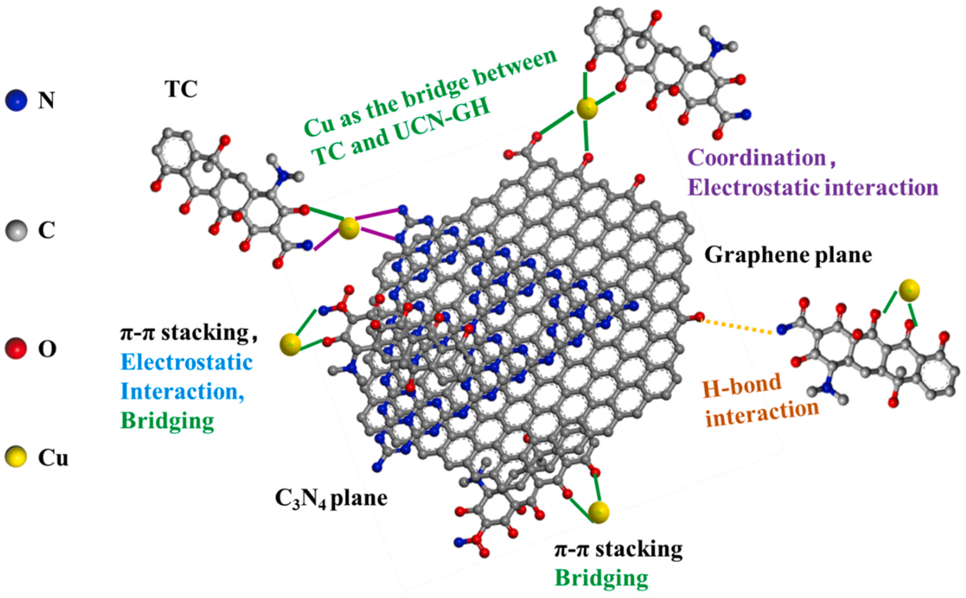

Fig. 6. Proposed mechanism for co-adsorption of tetracycline (TC) and Cu(II) on UCN-GH.

or graphene plane can also supply strong π-π interactions with organic compounds (Wang et al., 2014). Therefore, the adsorption of Cu(II) by UCN-GH was mainly attributed to electrostatic interaction as well as coordination with the acidic groups (e.g., -COOH and -OH) on reduced graphene oxide (Zhao et al., 2019), and N atoms on UCN (Cai et al., 2017). Whereas the strong π-π interactions between benzene rings in TC molecules and bulk π systems on UCN-GH surfaces, as well as the hydrogen bond interactions between -OH, -COOH, and -NH_2 probably play the major roles in TC adsorption (Zhao et al., 2019; Zhang et al., 2020). When Cu(II) and TC are co-existed, Cu(II) is likely to act as a bridge between TC and the adsorbent, and hence enhanced TC adsorption markedly (Ling et al., 2013, 2018; Zhao et al., 2019; Jia et al., 2016). On the contrary, TC did not obviously affect Cu removal because the adsorption of Cu on UCN-GH was mainly dependent on the stable coordination with amine/oxygen-functional groups. Therefore, the abundant functional groups and the bulk π systems of UCN-GH, as well as the bridging interaction between Cu(II) and TC contributed to the superhigh co-removal.

4. Conclusions

In summary, the hybrid UCN-GH hydrogels with a controlled macroporous network composed of well-dispersed UCN nanosheets incorporated with rGO nanosheets have been successfully fabricated using a facile hydrothermal method. In this strategy, the addition of UCN not only provided amine groups but also reduced the reduction of oxygen-functional groups on GO during the hydrothermal reaction, both of which can be severed as adsorption sites for Cu(II)/TC. The adsorption results in this study indicated that UCN-GH hydrogels have comparable high adsorption capacity for both Cu(II) and TC. Coordination and electrostatic interaction contribute to the adsorption of Cu(II) onto UCN-GH, while π-π interactions and hydrogen-bond interaction play dominant roles in TC adsorption. The co-exist of Cu(II) greatly promoted the TC adsorption due to its bridging effect. The co-adsorption capacity of this UCN-GH hydrogel has also been tested in the real river and STP effluent water, showing good feasibility for practical water application. Therefore, the highly effective adsorption of Cu(II) and TC, as well as their multi-pollutants indicated that UCN-GH has great potential for the removal of antibiotics and heavy metals from aquatic environments.

CRediT authorship contribution statement

Yiping Feng: Conceptualization, Validation, Investigation, Writing – original draft, Writing-review & editing, Visualization, Project administration, Funding acquisition. **Guang Chen, Yijian Zhang,** and **Daguang Li:** Methodology, Validation, Data curation. **Chen Ling:** Methodology, Data curation, Writing-review & editing. **Qiaoying Wang:** Formal analysis, Writing-review & editing. **Guoguang Liu:** Resources and Supervision.

Declaration of Competing Interest

The authors declare that they have no known competing financial interests or personal relationships that could have appeared to influence the work reported in this paper.

Acknowledgments

This work was supported by the National Natural Science Foundation of China (21707019), the Science and Technology Planning Project of Guangzhou City (201804010396), the Natural Science Foundation of Guangdong Province (2021A1515010019), the Characteristic Innovation Project of High Education Department of Guangdong Province (2017KTSCX058), State Key Laboratory of Pollution Control and Resource Reuse Foundation (PCRRF18015), and the Undergraduate Student's Innovative Practice Program of Guangdong University of Technology (xj202111845667). C.L. acknowledges funding support from the National Natural Science Foundation of China (51708281).

Associated content

The following is Supplementary data to this article: Fig. S1-S8, Table S1-S8.

Appendix A. Supporting information

Supplementary data associated with this article can be found in the online version at doi:10.1016/j.jhazmat.2021.127362.

References

Cai, X.G., He, J.Y., Chen, L., Chen, K., Li, Y.L., Zhang, K.S., Jin, Z., Liu, J.Y., Wang, C.M., Wang, X.G., Kong, L.T., Liu, J.H., 2017. A 2D-g-C3N4 nanosheet as an eco-friendly adsorbent for various environmental pollutants in water. Chemosphere 171, 192–201.

Chen, Y.J., Wang, F.H., Duan, L.C., Yang, H., Gao, J., 2016. Tetracycline adsorption onto rice husk ash, an agricultural waste: Its kinetic and thermodynamic studies. J. Mol. Liq. 222, 487–494.

Ding, F., Yang, D., Tong, Z., Nan, Y., Wang, Y., Zou, X., Jiang, Z., 2017. Graphitic carbon nitride-based nanocomposites as visible-light driven photocatalysts for environmental purification. Environ. Sci. -Nano 4, 1455–1469.

Feng, Y., Liu, X., Huynh, K.A., McCaffery, J.M., Mao, L., Gao, S., Chen, K.L., 2017. Heteroaggregation of graphene oxide with nanometer-and micrometer-sized hematite colloids: Influence on nanohybrid aggregation and microparticle sedimentation. Environ. Sci. Technol. 51, 6821–6828.

Feng, Y.P., Huynh, K.A., Xie, Z.J., Liu, G.G., Gao, S.X., 2019. Heteroaggregation and sedimentation of graphene oxide with hematite colloids: influence of water constituents and impact on tetracycline adsorption. Sci. Total Environ. 647, 708–715.

Ganiyu, S.O., van Hullebusch, E.D., Cretin, M., Esposito, G., Oturan, M.A., 2015. Coupling of membrane filtration and advanced oxidation processes for removal of pharmaceutical residues: a critical review. Sep. Purif. Technol. 156, 891–914.

Gao, H.C., Sun, Y.M., Zhou, J.J., Xu, R., Duan, H.W., 2013a. Mussel-inspired synthesis of polydopamine-functionalized graphene hydrogel as reusable adsorbents for water purification. ACS Appl. Mater. Interfaces 5, 425–432.

Gao, J., Liu, F.Q., Ling, P.P., Lei, J.T., Li, L.J., Li, C.H., Li, A.M., 2013b. High efficient removal of Cu(II) by a chelating resin from strong acidic solutions: complex formation and DFT certification. Chem. Eng. J. 222, 240–247.

Gao, Y., Li, Y., Zhang, L., Huang, H., Hu, J.J., Shah, S.M., Su, X.G., 2012. Adsorption and removal of tetracycline antibiotics from aqueous solution by graphene oxide. J. Colloid Interface Sci. 368, 540–546.

Han, Q.F., Zhao, S., Zhang, X.R., Wang, X.L., Song, C., Wang, S.G., 2020. Distribution, combined pollution and risk assessment of antibiotics in typical marine aquaculture farms surrounding the Yellow Sea, North China. Environ. Int 138, 105551.

Hu, R., Wang, X.K., Dai, S.Y., Shao, D.D., Hayat, T., Alsaedi, A., 2015. Application of graphitic carbon nitride for the removal of Pb(II) and aniline from aqueous solutions. Chem. Eng. J. 260, 469–477.

Huang, B., Liu, Y., Li, B., Liu, S., Zeng, G., Zeng, Z., Wang, X., Ning, Q., Zheng, B., Yang, C., 2017. Effect of Cu (II) ions on the enhancement of tetracycline adsorption by Fe_3O_4@ SiO_2-Chitosan/graphene oxide nanocomposite. Carbohyd. Polym. 157, 576–585.

Jia, D.-A., Zhou, D.-M., Wang, Y.-J., Zhu, H.-W., Chen, J.-L., 2008. Adsorption and cosorption of Cu (II) and tetracycline on two soils with different characteristics. Geoderma 146, 224–230.

Jia, S.Y., Yang, Z., Yang, W.B., Zhang, T.T., Zhang, S.P., Yang, X.Z., Dong, Y.Y., Wu, J.Q., Wang, Y.P., 2016. Removal of Cu(II) and tetracycline using an aromatic rings-functionalized chitosan-based flocculant: enhanced interaction between the flocculant and the antibiotic. Chem. Eng. J. 283, 495–503.

Jiang, W.J., Luo, W.J., Zong, R.L., Yao, W.Q., Li, Z.P., Zhu, Y.F., 2016. Polyaniline/carbon nitride nanosheets composite hydrogel: a separation-free and high-efficient photocatalyst with 3D hierarchical structure. Small 12, 4370–4378.

Kang, J., Liu, H., Zheng, Y.-M., Qu, J., Chen, J.P., 2010. Systematic study of synergistic and antagonistic effects on adsorption of tetracycline and copper onto a chitosan. J. Colloid Interface Sci. 344, 117–125.

Khan, A., Szulejko, J.E., Kim, K.H., Sammadar, P., Lee, S.S., Yang, X., Ok, Y.S., 2019a. A comparison of figure of merit (FOM) for various materials in adsorptive removal of benzene under ambient temperature and pressure. Environ. Res 168, 96–108.

Khan, A., Szulejko, J.E., Samaddar, P., Kim, K.H., Liu, B.T., Maitlo, H.A., Yang, X., Ok, Y. S., 2019b. The potential of biochar as sorptive media for removal of hazardous benzene in air. Chem. Eng. J. 361, 1576–1585.

Lam, K.F., Chen, X., McKay, G., Yeung, K.L., 2008. Anion effect on Cu^{2+} adsorption on NH_2-MCM-41. Ind. Eng. Chem. Res. 47, 9376–9383.

Li, Q., Ji, M., Li, X., Song, H., Wang, G., Qi, C., Li, A., 2019. Efficient co-removal of copper and tetracycline from aqueous solution by using permanent magnetic cation exchange resin. Bioresour. Technol. 293, 122068.

Ling, C., Liu, F.Q., Xu, C., Chen, T.P., Li, A.M., 2013. An integrative technique based on synergistic coremoval and sequential recovery of copper and tetracycline with dual-functional chelating resin: roles of amine and carboxyl groups. ACS Appl. Mater. Interfaces 5, 11808–11817.

Ling, C., Yue, C.L., Liu, F.Q., Wei, M.M., Chen, T.P., Zhu, J.J., 2018. Contrastive study for coadsorption of copper and two dihydroxybenzene isomers by a multi-amine modified resin. J. Hazard Mater. 352, 47–56.

Liu, K., Sun, M.M., Ye, M., Chao, H.Z., Zhao, Y.C., Xia, B., Jiao, W.T., Feng, Y.F., Zheng, X.X., Liu, M.Q., Jiao, J.G., Hu, F., 2019. Coexistence and association between heavy metals, tetracycline and corresponding resistance genes in vermicomposts originating from different substrates. Environ. Pollut. 244, 28–37.

Luo, H., Liu, Y., Lu, H., Fang, Q., Rong, H., 2021. Efficient adsorption of tetracycline from aqueous solutions by modified alginate beads after the removal of Cu (II) ions. ACS Omega 6, 6240–6251.

Ma, Y.F., Qi, Y., Yang, L., Wu, L., Li, P., Gao, F., Qi, X.B., Zhang, Z.L., 2021. Adsorptive removal of imidacloprid by potassium hydroxide activated magnetic sugarcane bagasse biochar: adsorption efficiency, mechanism and regeneration. J. Clean. Prod. 292, 126005.

Marcano, D.C., Kosynkin, D.V., Berlin, J.M., Sinitskii, A., Sun, Z.Z., Slesarev, A., Alemany, L.B., Lu, W., Tour, J.M., 2010. Improved synthesis of graphene oxide. ACS Nano 4, 4806–4814.

Mishra, S., Bharagava, R.N., More, N., Yadav, A., Zainith, S., Mani, S., Chowdhary, P., 2019. Heavy metal contamination: an alarming threat to environment and human health. In: Environmental Biotechnology: For Sustainable Future. Springer, pp. 103–125.

Nie, T., Hao, P., Zhao, Z., Zhou, W., Zhu, L., 2019. Effect of oxidation-induced aging on the adsorption and co-adsorption of tetracycline and Cu^{2+} onto biochar. Sci. Total Environ. 673, 522–532.

Ong, W.J., Tan, L.L., Ng, Y.H., Yong, S.T., Chai, S.P., 2016. Graphitic carbon nitride (g-C_3N_4)-based photocatalysts for artificial photosynthesis and environmental remediation: are we a step closer to achieving sustainability? Chem. Rev. 116, 7159–7329.

Parolo, M.E., Avena, M.J., Pettinari, G.R., Baschini, M.T., 2012. Influence of Ca^{2+} on tetracycline adsorption on montmorillonite. J. Colloid Interface Sci. 368, 420–426.

Peng, W.J., Li, H.Q., Liu, Y.Y., Song, S.X., 2017. A review on heavy metal ions adsorption from water by graphene oxide and its composites. J. Mol. Liq. 230, 496–504.

Poole, K., 2017. At the nexus of antibiotics and metals: the impact of Cu and Zn on antibiotic activity and resistance. Trends Microbiol 25, 820–832.

Qin, Q., Wu, X., Chen, L., Jiang, Z., Xu, Y., 2018. Simultaneous removal of tetracycline and Cu (II) by adsorption and coadsorption using oxidized activated carbon. RSC Adv. 8, 1744–1752.

Repo, E., Warchol, J.K., Bhatnagar, A., Mudhoo, A., Sillanpaa, M., 2013. Aminopolycarboxylic acid functionalized adsorbents for heavy metals removal from water. Water Res. 47, 4812–4832.

Rodriguez-Mozaz, S., Chamorro, S., Marti, E., Huerta, B., Gros, M., Sanchez-Melsio, A., Borrego, C.M., Barcelo, D., Balcazar, J.L., 2015. Occurrence of antibiotics and antibiotic resistance genes in hospital and urban wastewaters and their impact on the receiving river. Water Res. 69, 234–242.

Saadi, R., Saadi, Z., Fazaeli, R., Fard, N.E., 2015. Monolayer and multilayer adsorption isotherm models for sorption from aqueous media. Korean J. Chem. Eng. 32, 787–799.

Schwarzenbach, R.P., Escher, B.I., Fenner, K., Hofstetter, T.B., Johnson, C.A., von Gunten, U., Wehrli, B., 2006. The challenge of micropollutants in aquatic systems. Science 313, 1072–1077.

Song, L.Z., Zhao, X.D., Fu, J., Wang, X.L., Sheng, Y.P., Liu, X.W., 2012. DFT investigation of Ni(II) adsorption onto MA-DTPA/PVDF chelating membrane in the presence of coexistent cations and organic acids. J. Hazard. Mater. 199, 433–439.

Tong, Z.W., Yang, D., Shi, J.F., Nan, Y.H., Sun, Y.Y., Jiang, Z.Y., 2015. Three-dimensional porous aerogel constructed by g-C_3N_4 and graphene oxide nanosheets with excellent visible-light photocatalytic performance. ACS Appl. Mater. Interfaces 7, 25693–25701.

Wang, F.L., Wang, Y.F., Li, Y.Y., Cui, X.H., Zhang, Q.X., Xie, Z.J., Liu, H.J., Feng, Y.P., Lv, W.Y., Liu, G.G., 2018a. The facile synthesis of a single atom-dispersed silver-modified ultrathin g-C_3N_4 hybrid for the enhanced visible-light photocatalytic degradation of sulfamethazine with peroxymonosulfate. Dalton Trans. 47, 6924–6933.

Wang, F.L., Wang, Y.F., Feng, Y.P., Zeng, Y.Q., Xie, Z.J., Zhang, Q.X., Su, Y.H., Chen, P., Liu, Y., Yao, K., Lv, W.Y., Liu, G.G., 2018b. Novel ternary photocatalyst of single atom-dispersed silver and carbon quantum dots co-loaded with ultrathin g-C_3N_4 for broad spectrum photocatalytic degradation of naproxen. Appl. Catal. B-Environ. 221, 510–520.

Wang, J., Chen, Z.M., Chen, B.L., 2014. Adsorption of polycyclic aromatic hydrocarbons by graphene and graphene oxide nanosheets. Environ. Sci. Technol. 48, 4817–4825.

Wang, J., Yue, D., Cui, D., Zhang, L., Dong, X., 2021a. Insights into adsorption of humic substances on graphitic carbon nitride. Environ. Sci. Technol. 55, 7910–7919.

Wang, J.L., Zhuan, R., 2020. Degradation of antibiotics by advanced oxidation processes: an overview. Sci. Total Environ. 701, 135023.

Wang, R.-Z., Huang, D.-L., Liu, Y.-G., Zhang, C., Lai, C., Wang, X., Zeng, G.-M., Zhang, Q., Gong, X.-M., Xu, P., 2020. Synergistic removal of copper and tetracycline from aqueous solution by steam-activated bamboo-derived biochar. J. Hazard. Mater. 384, 121470.

Wang, S.F., Li, X., Liu, Y.G., Zhang, C., Tan, X.F., Zeng, G.M., Song, B.A., Jiang, L.H., 2018c. Nitrogen-containing amino compounds functionalized graphene oxide: synthesis, characterization and application for the removal of pollutants from wastewater: a review. J. Hazard. Mater. 342, 177–191.

Wang, T., Zhang, J., Tao, M.T., Xu, C.M., Chen, M., 2021b. Quantitative characterization of toxicity interaction within antibiotic-heavy metal mixtures on *Chlorella pyrenoidosa* by a novel area-concentration ratio method. Sci. Total Environ. 762, 144180.

Wang, X., Liang, Y.H., An, W.J., Hu, J.S., Zhu, Y.F., Cui, W.Q., 2017. Removal of chromium (VI) by a self-regenerating and metal free g-C_3N_4/graphene hydrogel system via the synergy of adsorption and photo-catalysis under visible light. Appl. Catal. B-Environ. 219, 53–62.

Wang, X.C., Chen, X.F., Thomas, A., Fu, X.Z., Antonietti, M., 2009. Metal-containing carbon nitride compounds: a new functional organic-metal hybrid material. Adv. Mater. 21, 1609–1612.

Wang, Y., Wang, X., Li, J., Li, Y., Xia, S., Zhao, J., Minale, T.M., Gu, Z., 2019. Coadsorption of tetracycline and copper (II) onto struvite loaded zeolite–an environmentally friendly product recovered from swine biogas slurry. Chem. Eng. J. 371, 366–377.

Wang, Y.J., Jia, D.A., Sun, R.J., Zhu, H.W., Zhou, D.M., 2008. Adsorption and cosorption of tetracycline and copper(II) on montmorillonite as affected by solution pH. Environ. Sci. Technol. 42, 3254–3259.

Xie, Z., Feng, Y., Wang, F., Chen, D., Zhang, Q., Zeng, Y., Lv, W., Liu, G., 2018. Construction of carbon dots modified $MoO_3/g\text{-}C_3N_4$ Z-scheme photocatalyst with enhanced visible-light photocatalytic activity for the degradation of tetracycline. Appl. Catal. B-Environ. 229, 96–104.

Xing, H.T., Chen, J.H., Sun, X., Huang, Y.H., Su, Z.B., Hu, S.R., Weng, W., Li, S.X., Guo, H.X., Wu, W.B., 2015. NH_2-rich polymer/graphene oxide use as a novel adsorbent for removal of Cu (II) from aqueous solution. Chem. Eng. J. 263, 280–289.

Xu, Y.X., Sheng, K.X., Li, C., Shi, G.Q., 2010. Self-assembled graphene hydrogel via a one-step hydrothermal process. ACS Nano 4, 4324–4330.

Xu, Z., Huang, W., Xie, H., Feng, X., Wang, S., Song, H., Xiong, J., Mailhot, G., 2021. Co-adsorption and interaction mechanism of cadmium and sulfamethazine onto activated carbon surface. Colloids Surf. A Physicochem. Eng. Asp. 619, 126540.

Yang, W.B., Zheng, F.F., Lu, Y.P., Xue, X.X., Li, N., 2011. Adsorption interaction of tetracyclines with porous synthetic resins. Ind. Eng. Chem. Res. 50, 13892–13898.

Yang, Z., Jia, S.Y., Zhang, T.T., Zhuo, N., Dong, Y.Y., Yang, W.B., Wang, Y.P., 2015. How heavy metals impact on flocculation of combined pollution of heavy metals-antibiotics: a comparative study. Sep. Purif. Technol. 149, 398–406.

Yousefi, N., Lu, X.L., Elimelech, M., Tufenkji, N., 2019. Environmental performance of graphene-based 3D macrostructures. Nat. Nanotechnol. 14, 107–119.

Zeng, X.K., McCarthy, D.T., Deletic, A., Zhang, X.W., 2015. Silver/reduced graphene oxide hydrogel as novel bactericidal filter for point-of-use water disinfection. Adv. Funct. Mater. 25, 4344–4351.

Zhang, J.L., Zhai, J.R., Zheng, H., Li, X.Y., Wang, Y.R., Li, X.P., Xing, B.S., 2020. Adsorption, desorption and coadsorption behaviors of sulfamerazine, Pb (II) and benzoic acid on carbon nanotubes and nano-silica. Sci. Total Environ. 738, 139685.

Zhang, Y., Cai, X.Y., Lang, X.M., Qiao, X.L., Li, X.H., Chen, J.W., 2012. Insights into aquatic toxicities of the antibiotics oxytetracycline and ciprofloxacin in the presence of metal: complexation versus mixture. Environ. Pollut. 166, 48–56.

Zhang, Y.H., Zhu, C.Q., Liu, F.Q., Yuan, Y., Wu, H.D., Li, A.M., 2019. Effects of ionic strength on removal of toxic pollutants from aqueous media with multifarious adsorbents: a review. Sci. Total Environ. 646, 265–279.

Zhao, C., Hong, P., Li, Y., Song, X., Wang, Y., Yang, Y., 2019. Mechanism of adsorption of tetracycline–Cu multi-pollutants by graphene oxide (GO) and reduced graphene oxide (rGO). J. Chem. Technol. Biot. 94, 1176–1186.

Zhu, Z., Zhang, M., Wang, W., Zhou, Q., Liu, F., 2018. Efficient and synergistic removal of tetracycline and Cu (II) using novel magnetic multi-amine resins. Sci. Rep. 8, 1–9.